

# Formation of superheavy elements in heavy-ion collisions

V.Yu. Denisov<sup>1,2</sup>

<sup>1</sup> Gesellschaft für Schwerionenforschung, D-64291 Darmstadt, Germany

<sup>2</sup> Institute for Nuclear Research, 03680 Kiev, Ukraine

The cold fusion reactions related to  $^{208}\text{Pb}$  and  $^{209}\text{Bi}$  targets leading to superheavy elements (SHE) with  $Z=104-112$  have been successfully considered in our model recently [2]. Here we briefly discuss this model and extend our consideration to fusion reactions between similar target and projectile. The reactions between weakly deformed target close to Pb and  $^{76}\text{Ge}$ ,  $^{82}\text{Se}$  projectiles are also studied. The available experimental cross-sections are well described. The nucleus-nucleus interaction potential for reactions leading to SHEs are shortly discussed.

## I. INTRODUCTION

The synthesis of superheavy elements (SHEs) was and still is an outstanding research object. The properties of SHEs are studied both theoretically and experimentally [1-7]. In the cold fusion, SHEs are produced by reactions of the type  $X+(\text{Pb,Bi}) \rightarrow \text{SHE}+1n$  at subbarrier energies [1]. The excitation energy of a compound nucleus formed by cold fusion is low,  $\approx 10-20$  MeV [1]. The experimental study of an excitation function for the SHE production becomes increasingly difficult due to very small cross-sections and narrow width of the excitation function [1].

In Refs. [2,3] we present a model for description of measured excitation functions for the SHE production in the cold fusion reactions. The maximum position and the width of the excitation function for cold fusion reactions  $X+^{208}\text{Pb}, ^{209}\text{Bi}$  leading to elements with  $Z=104-112$  are well described in [2] (see also Figs. 1,3,4). Within our approach [2] the process of the SHE formation proceeds in three stages: (i.) The capture of two spherical nuclei and the formation of a common shape of the two touching nuclei. Low-energy surface vibrations and a transfer of few nucleons are taken into account at the first step of the reaction. (ii.) The formation of a spherical or near spherical compound nucleus. (iii.) The surviving of an excited compound nucleus during evaporation of neutrons and  $\gamma$ -ray emission which compete with fission. A reduction of the fission barrier is taken into account, which arises from a reduction of the shell effects at increasing excitation energy of the compound nucleus.

One of the heaviest systems experimentally studied over a wider range of excitation energy is  $^{58}\text{Fe}+^{208}\text{Pb} \rightarrow ^{265}\text{Hs}+n$  [1], the data are shown in Fig. 1. The experimental data are compared with several modifications of our model. In the simplest case, using tunneling through a one-dimensional barrier and the WKB method, the model strongly underestimates the experimental fusion cross-sections. Better agreement is obtained, when the neutron transfer channels from lead to iron are taken into account. Similarly, the cross-sections increase if the low-energy  $2^+$  and  $3^-$  surface vibrational excitations of both projectile and target are included in the calculations, see Fig. 1. The best fits are obtained by considering transfer and vibrations simultaneously. The values of parameters and other details are presented in Ref. [2]. In our model [2] we have two fitting parameters as well as other parameters, which are taken from experimental data and from other calculations, see for detail [2]. Note that we are able to describe data for reactions  $^{58}\text{Fe}+^{207}\text{Pb} \rightarrow ^{264}\text{Hs}+n$  (see Fig. 1) and  $^{58}\text{Fe}+^{209}\text{Bi} \rightarrow ^{266}\text{Mt}+n$  (see Fig. 11 in [2]) by using the same fitting parameters as fixed for reaction  $^{58}\text{Fe}+^{208}\text{Pb} \rightarrow ^{265}\text{Hs}+n$ .

The results of similar calculations for reactions  $^{50}\text{Ti}+^{208}\text{Pb} \rightarrow ^{257}\text{Rf}+n$ ,  $^{62,64}\text{Ni}+^{207,208,210}\text{Pb} \rightarrow ^{110}+n$ , and  $^{54}\text{Cr}+^{208}\text{Pb} \rightarrow ^{261}\text{Sg}+n$  are also presented in Figs. 1,3,4. Our calculation for reaction  $^{50}\text{Ti}+^{208}\text{Pb} \rightarrow ^{257}\text{Rf}+n$  is well agreed with the experimental data for low collision energies, see Fig. 1. Note that the threshold of  $2n$  evaporation channel is near 186 MeV. We have not take into account the emission of the second neutron, which should reduce the difference between our calculations and experimental data for energies close to 186-188 MeV.

## II. PRODUCTION OF SHE IN NEARLY SYMMETRIC HEAVY ION COLLISIONS

It is also possible to produce SHE in collisions of similar nuclei. For example, the nuclide  $^{265}\text{Hs}$  can be formed in both reactions  $^{58}\text{Fe}+^{208}\text{Pb} \rightarrow ^{265}\text{Hs}+n$  and  $^{130}\text{Xe}+^{136}\text{Xe} \rightarrow ^{265}\text{Hs}+n$ . The excitation functions for reactions  $^{130,136}\text{Xe}+^{136}\text{Xe} \rightarrow ^{265,271}\text{Hs}+n$  obtained in our model for different values of the inner barrier  $B_{\text{Sph}} = 6$  MeV and 14 MeV are presented in Fig. 1. The inner barrier is the barrier appearing during the shape evolution from two touching nuclei to the compound nucleus [2,3]. The shape evolution stage is related with the second step of the SHE formation.

We can describe the touching configuration and shape evolution of nearly symmetric systems by using the shape parametrization  $R(\vartheta) = R(p, q)[1 + p \sum_{\ell=2, \ell \neq 4}^9 \beta_{\ell}^t Y_{\ell 0}(\vartheta) + q \beta_4^t Y_{40}(\vartheta)]$ , where  $p = q = 1$  at the touching point of two

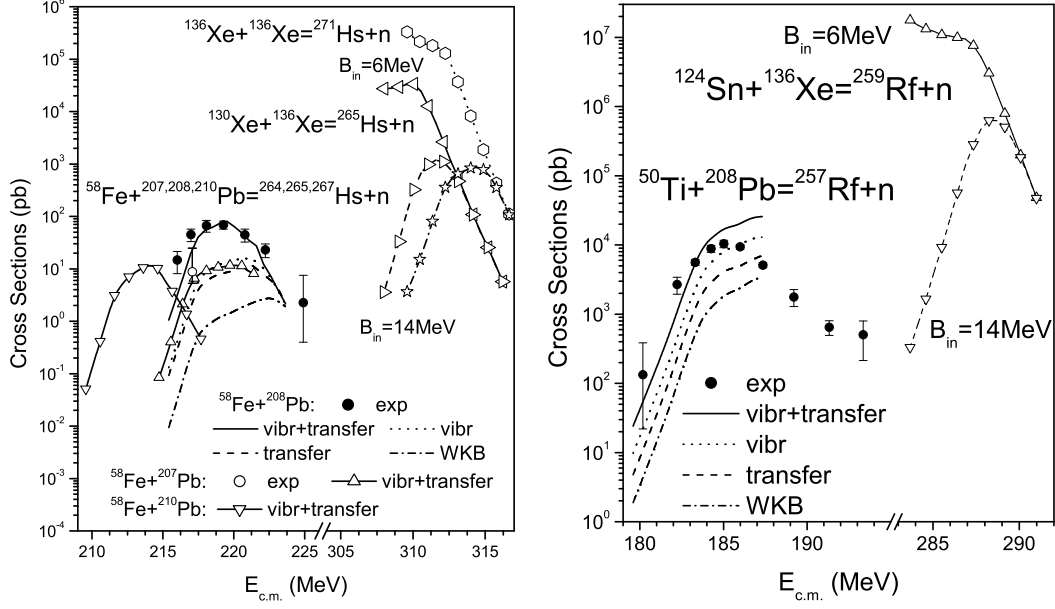


FIG. 1. Calculated excitation functions for reactions  $^{58}\text{Fe} + ^{207,208,210}\text{Pb} \rightarrow ^{264,265,267}\text{Hs} + n$  (left),  $^{130,136}\text{Xe} + ^{136}\text{Xe} \rightarrow ^{265,271}\text{Hs} + n$  (left),  $^{50}\text{Ti} + ^{208}\text{Pb} \rightarrow ^{257}\text{Rf} + n$  (right) and  $^{124}\text{Sn} + ^{136}\text{Xe} \rightarrow ^{259}\text{Rf} + n$  (right). For reactions  $^{58}\text{Fe} + ^{208}\text{Pb} \rightarrow ^{265}\text{Hs} + n$  and  $^{50}\text{Ti} + ^{208}\text{Pb} \rightarrow ^{257}\text{Rf} + n$  the solid curves take into account both the low-energy  $2^+$  and  $3^-$  vibrations and the neutrons transfer channels. The dotted and the dashed curves for these reactions show the results based on solely the  $2^+$  and  $3^-$  vibrations and the neutron transfer channels, respectively. The results of the one-dimensional WKB approach for these reactions are shown by the dash-dotted curves. Calculations including both vibrations and transfer enhancements obtained for  $^{130,136}\text{Xe} + ^{136}\text{Xe} \rightarrow ^{265,271}\text{Hs} + n$  and  $^{124}\text{Sn} + ^{136}\text{Xe} \rightarrow ^{259}\text{Rf} + n$  reactions are additionally marked by symbols, see assignments. The experimental data are taken from [1,4].

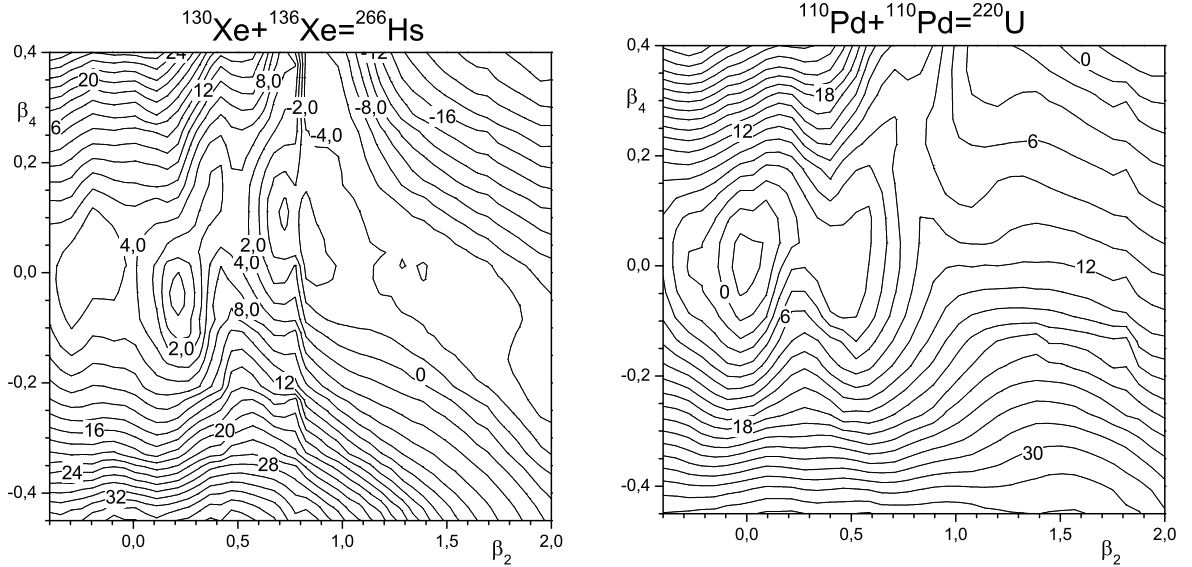


FIG. 2. Potential energy surfaces as a function of the deformation parameters  $\beta_2$  and  $\beta_4$  for cold fusion reactions  $^{130}\text{Xe} + ^{136}\text{Xe} \rightarrow ^{266}\text{Hs}$  (left) and  $^{110}\text{Pd} + ^{110}\text{Pd} \rightarrow ^{220}\text{U}$  (right). Parameters  $\beta_\ell$  are equal to:  $\beta_2 = p\beta_2^t$ ,  $\beta_4 = q\beta_4^t$ . The touching configurations of the spherical projectile and target nuclei are close to the bottom right corner of each map and that of the ground-states are close to  $\beta_2 \approx 0.2(0.0)$  and  $\beta_4 \approx -0.05(0.0)$  for  $^{266}\text{Hs}$  ( $^{220}\text{U}$ ). The contour lines are drawn every 2 MeV.

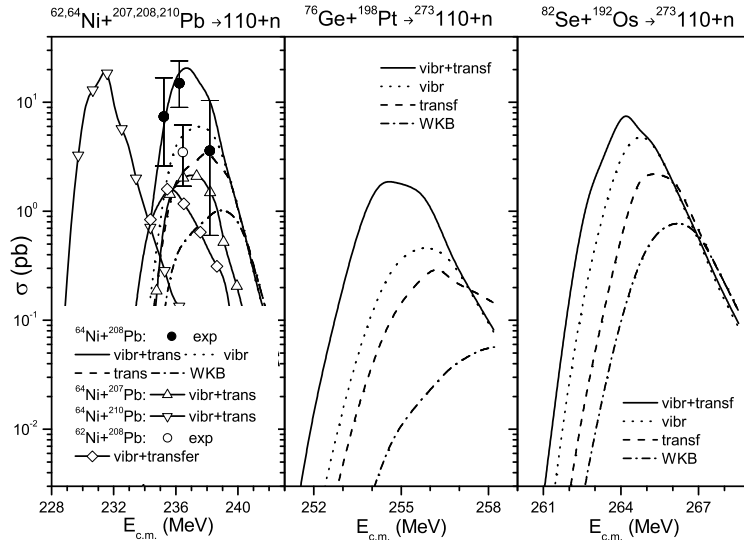


FIG. 3. Calculated excitation functions for the reactions  $^{62,64}\text{Ni}+^{207,208,210}\text{Pb} \rightarrow 110+n$  (left),  $^{76}\text{Ge}+^{198}\text{Pt} \rightarrow ^{273}110+n$  (middle) and  $^{82}\text{Se}+^{192}\text{Os} \rightarrow ^{273}110+n$  (right). The solid curve takes into account both the low-energy  $2^+$  and  $3^-$  vibrations and the neutron transfer channels. The dashed, dotted and dash-dotted lines show the results of similar calculations as for reaction  $^{58}\text{Fe}+^{208}\text{Pb} \rightarrow ^{265}\text{Hs}+n$  in Fig. 1. The experimental data are taken from [1].

spherical colliding ions and the deformation parameters  $\beta_\ell^t$  are fixed at the touching point. This parametrization of the nuclear shape near touching point is very accurate for symmetric case. The volume of the nucleus is constant during the shape evolution. The potential energy surfaces for reactions  $^{130}\text{Xe}+^{136}\text{Xe} \rightarrow ^{266}\text{Hs}$  and  $^{110}\text{Pd}+^{110}\text{Pd} \rightarrow ^{220}\text{U}$  are presented in Fig. 2.

As mentioned above, we made calculations of synthesis of the SHE using nearly symmetric reactions for two different values of the inner barrier. The value of the inner barrier  $B_{\text{Sph}} = 6$  MeV is near the adiabatic fission barrier, see Fig. 2. Note that the potential energy surface for  $^{266}\text{Hs}$  in Fig. 2 has a strong slope from touching point (bottom right corner) to the quasi-fission direction (upper right corner). It is possible to evaluate exact value of the inner barrier and the branching ratio between compound nucleus formation and quasi-fission processes by studying the quantum dynamical shape evolution from two touching nuclei to the near spherical compound nucleus. Unfortunately such calculations are not available now. Therefore, we also made calculations for a higher value of the inner barrier  $B_{\text{Sph}} = 14$  MeV, which may simulate a stronger competition between the SHE formation and the quasi-fission. Note that the SHE production cross sections for near symmetric reactions in the case of  $k \geq 1$  neutrons evaporation are mainly related to the shape evolution stage, because the height of the outer (capture) barrier is smaller than collision energies.

Nucleus  $^{220}\text{U}$  is the heaviest nucleus, which have been formed in symmetric reaction  $^{110}\text{Pd} + ^{110}\text{Pd} \rightarrow ^{220}\text{U}$  [8]. The landscape of potential energy surface for Pd+Pd reaction has much stronger repulsion at touching point region than the one for Xe+Xe reaction, see fig. 2. Due to this the fusion trajectory for Pd+Pd reaction at low energies should strongly deviates to  $\beta_4 \approx 0$  near touching point or penetrates through the thick barrier near  $\beta_2 \approx 1.0 \div 1.7$  and  $\beta_4 \approx -0.4 \div -0.25$ . So the SHE production is reduced in both cases. Nevertheless the cross section for reaction  $^{110}\text{Pd} + ^{110}\text{Pd} \rightarrow ^{220}\text{U}$  at lowest energy close to 1 nb [8]. We may expect that near symmetric reactions as Sn+Xe or Xe+Xe very attractive tools to produce SHEs, because they have thin barrier near  $\beta_2 \approx 0.5 \div 0.8$ ,  $\beta_4 \approx -0.4 \div 0.05$  and absence of strong repulsion near the touching point.

### III. REACTION WITH GE AND SE PROJECTILES

Reactions with targets slightly lighter than Pb are also interesting for studying too. The reactions between  $^{76}\text{Ge}+^{198}\text{Pt} \rightarrow ^{273}110+n$ ,  $^{82}\text{Se}+^{192}\text{Os} \rightarrow ^{273}110+n$ ,  $^{76}\text{Ge}+^{186}\text{W} \rightarrow ^{261}\text{Sg}+n$  and  $^{82}\text{Se}+^{180}\text{Hf} \rightarrow ^{261}\text{Sg}+n$  are compared with the cold fusion reactions leading to the same SHE in Figs. 3,4.

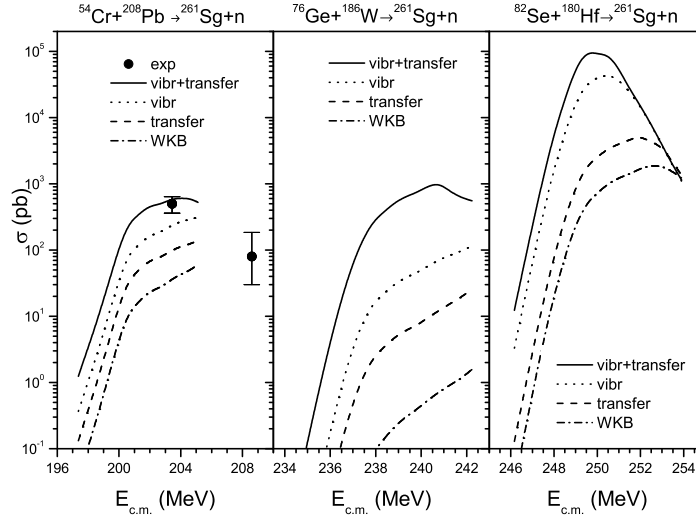


FIG. 4. Calculated excitation functions for the reactions  $^{54}\text{Cr}+^{208}\text{Pb} \rightarrow ^{261}\text{Sg}+n$  (left),  $^{76}\text{Ge}+^{186}\text{W} \rightarrow ^{261}\text{Sg}+n$  (middle) and  $^{82}\text{Se}+^{180}\text{Hf} \rightarrow ^{261}\text{Sg}+n$  (right). The line assignments are the same as in Fig. 3. The experimental data are taken from [1].

Note that our code is proposed for the evaluation of the SHE production cross section in fusion of two spherical nuclei [2]. However we may simulate static deformation effect in deformed target by taking the same value of the vibration  $2^+$  amplitude as the value of static quadrupole deformation. We also equate the energy of the first  $2^+$  vibration state to the value of the first rotational  $2^+$  state in deformed nuclei.

Reactions with  $^{76}\text{Ge}$  and  $^{82}\text{Se}$  projectiles in Figs. 3,4 are strongly enhanced by coupling to both neutron transfer and low-energy surface vibrations. More symmetric reactions with  $^{82}\text{Se}$  projectile have smaller difference between the capture barrier height and the ground state  $q$ -value energy of compound nucleus formed at fusion. Due to this, the SHE production cross sections for reactions with Se projectile are higher than the one for Ge case, see Figs. 3,4.

#### IV. INTERACTION POTENTIAL BETWEEN VERY HEAVY NUCLEI

The ion-ion potential near and before the touching point is quite differently treated in models [2-3,5-7]. Note that the interaction potential between very heavy ions near the touching point is not well known, because there are not so many experimental data for such cases. The knowledge of the ion-ion potential near touching point is crucial for the capture stage of the SHE production. The uncertainty of the interaction potential between heavy ions near the touching point gives possibility for very different proposals on the mechanisms of the SHEs formation [2-3,5-7]. So, there is necessity to reduce the uncertainty of the interaction potential values near the touching point.

We calculate the interaction potential between heavy ions around the touching point for various Skyrme forces in the extended Thomas-Fermi (ETF) approximation by using the frozen Hartree-Fock-Bogoliubov densities of the individual nuclei [13]. In Fig. 5 we present the interaction potentials between  $^{70}\text{Zr}$  and  $^{208}\text{Pb}$  evaluated in the ETF approximation with different parameter sets of the Skyrme force. The potentials obtained by using different analytical expressions [9–12] are also shown in Fig. 5. The potentials obtained in the ETF frozen approximation with different parameter sets of the Skyrme force have very close values of both the barrier heights and the barrier distances. The ion-ion potentials evaluated for SkM\*, SkP and SLy4 sets are very close to each other at all distances presented in Fig. 5. However Sk3 parameter set of the Skyrme force has largest value of the compressibility among all considered here sets of the Skyrme force. Due to this the repulsion between ions at small distances related with the volume of overlapped ions densities is strongest in the case of Sk3 set of the Skyrme force.

The potential wells obtained in the ETF approximation are shallow, see Fig. 5. The minimal value of the potential well is located at the distance smaller than the touching point distance of two spherical ions, which is close to 12 fm. Here we roughly determined touching point distance as  $R = r_0(A_1^{1/3} + A_2^{1/3})$ , where  $r_0 = 1.2$  fm. Therefore both processes, the capture of two ions and the neck formation, are taken place in the potential well. The barriers obtained with the help of different analytical expressions for ion-ion potential [9–12] are spread in very wide interval in Fig. 5.

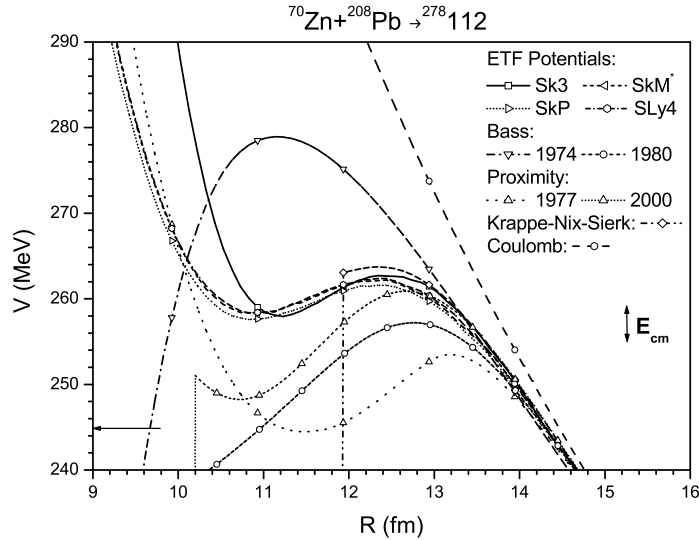


FIG. 5. The potentials for the collision  $^{70}\text{Zr} + ^{208}\text{Pb}$  evaluated in the ETF approximation with Sk3, SkM\*, SkP and SLy4 parameter sets of the Skyrme force are given. The Coulomb potential and the potentials obtained in the two versions (1974 and 1980 years) of the Bass parametrization [11], in the KNS parametrization [12] and in two versions of proximity approximation (1977 and 2000 years) [9,10] are also presented. The range of collision energies in the middle of the target used in experiments [1] is marked by vertical arrow in the right part. The ground state reaction Q-value related with the formation of compound nucleus  $^{278}112$  is marked by the horizontal arrow in the left bottom corner.

The further studies shows that the potentials between light and medium heavy ions have deep and wide capture well. The depth of these well decrease with increasing  $Z_1Z_2$  and disappear for very heavy colliding ions [13]. Due to this the capture process is suppressed for the case of reactions between extremely heavy ions.

Concluding, we note that it would be interesting to check experimentally our estimates for both symmetric reactions and reactions with  $^{76}\text{Ge}$  and  $^{82}\text{Se}$  projectiles.

The author would like to thank S. Hofmann, V. Ninov, W. Nörenberg and J. Peter for useful discussions. He acknowledges gratefully support from ISOL'2001 Organizing Committee of the Conference and GSI.

- 
- [1] S. Hofmann and G. Münzenberg, *Rev. Mod. Phys.* **72**, 733 (2000).  
 [2] V.Yu. Denisov and S. Hofmann, *Phys. Rev.* **C61**, 034606 (2000).  
 [3] V.Yu. Denisov, *Prog. Part. Nucl. Phys.* **46**, 303 (2001); *Proc. Tours Symposium on Nuclear Physics IV*, Tours, France, September 2000, *AIP Conference Proceedings* **561**, 433 (2001); *Proc. Int. Workshop on Fusion Dynamics at the Extremes*, Dubna, May 2000, *World Scientific*, Singapore, p. 203 (2001).  
 [4] V. Ninov, (private communications).  
 [5] R. Smolanczuk, *Phys. Rev.* **C56**, 812 (1997); *Phys. Rev.* **C59**, 2634 (1999); *Phys. Rev.* **C63**, 044607 (2001).  
 [6] E. Cherepanov, *Pramana* **53**, 619 (1999); G.S. Giardina, S. Hofmann, A.I. Muminov and A.K. Nasirov, *Eur. Phys. J.* **A8**, 205 (2000); G.G. Adamian, N.V. Antonenko and W. Scheid, *Nucl. Phys.* **A678**, 24 (2000).  
 [7] Y. Aritomo, T. Wada, M. Ohta, and Y. Abe, *Phys. Rev.* **C59**, 796 (1999).  
 [8] W. Morawek, *et al.*, *Z. Phys.* **A341**, 75 (1991).  
 [9] J. Blocki, J. Randrup, W.J. Swiatecki, C.F. Tsang, *Ann. Phys.* **105**, (1977) 427.  
 [10] W.D. Myers, W.J. Swiatecki, *Phys. Rev.* **62**, (2000) 044610.  
 [11] R. Bass, *Nuclear Reactions with Heavy Ions* (Springer-Verlag, Berlin 1980) 410.  
 [12] H.J. Krappe, J.R. Nix, A.J. Sierk, *Phys. Rev.* **C20**, (1979) 992.  
 [13] V.Yu. Denisov and W. Nörenberg, in preparation.